A Stable Dimer in the pH-Induced Equilibrium Unfolding of the Homo-Hexameric Enzyme 4-Oxalocrotonate Tautomerase (4-OT)†

Peter Silinski and Michael C. Fitzgerald*

Department of Chemistry, Duke University, Durham, North Carolina, 27708

Received October 2, 2001; Revised Manuscript Received December 21, 2001

ABSTRACT: 4-Oxalocrotonate tautomerase (4-OT) is a multimeric, bacterial enzyme comprised of 6 identical 62-amino acid subunits, which associate under native conditions to form a homo-hexameric structure stabilized entirely by noncovalent interactions. We have previously shown that the GuHCl-induced equilibrium unfolding of 4-OT at pH 8.5 is well modeled as a two-state process involving only hexamer and unfolded monomer; and we have obtained spectroscopic evidence that intermediate state(s) is (are) populated in the equilibrium unfolding reaction at pHs 6.0 and 7.4 [Silinski, P., Allingham, M. J., and Fitzgerald, M. C. (2001) *Biochemistry 40*, 4493−4502]. Here, we report on the pH-induced equilibrium unfolding of 4-OT using size-exclusion chromatography (SEC), far-UV-circular dichroism (CD) spectroscopy, and catalytic activity measurements over the pH range from 1.5 to 10.1. Our results indicate that the native hexamer of 4-OT is the predominant species in solution at pHs ≥6.2, that a partially folded dimeric state of 4-OT is stabilized in solution at pH 4.8, and that the enzyme is largely denatured in strongly acidic solutions (pH ≤3.1). GuHCl-induced equilibrium unfolding studies on 4-OT at pH 4.8 indicate that the folded 4-OT dimer populated at this pH is stabilized by 11.7 kcal·mol^{-1}. The results of biophysical studies on a fluorescent analogue of the enzyme, 4-OT(F50Y), and the results of UV photo-cross-linking studies on a synthetically derived 4-OT analogue, 4-OT(P1Bpa), suggest the polypeptide chains in the 4-OT dimer are nativelike in structure with the exception of their C-termini.

Multimeric enzymes constitute an important class of proteins found in biological systems. They are involved in a wide variety of biochemical processes such as respiration, metabolism, and gene regulation. However, relatively little is known about the folding and assembly of multimeric enzymes in vivo or in vitro. Much of what is currently understood about protein folding has been derived from studies on small, monomeric proteins and protein domains, or from studies of oligomeric proteins with no catalytic function (*1*−*5*). Several recent biophysical studies on multimeric enzyme systems have provided some insight into the folding and assembly reactions of oligomeric enzymes. In most cases, the unfolding transitions measured by catalytic activity precede those measured by other structural probes such as circular dichroism (CD) and fluorescence spectroscopy (*6*, *7*). This phenomenon has been attributed, in part, to an added flexibility in an enzyme's active site with respect to the overall protein (*8*, *9*). In many cases, the loss of an enzyme's catalytic function in denaturation experiments coincides with the formation of partially folded intermediates.

Inactive, partially folded monomers have been identified in equilibrium unfolding studies of several multimeric enzymes, such as the dimeric aspartate aminotransferase, the tetrameric lactate dehydrogenase, and the tetrameric pyruvate oxidase (*10*−*12*). A few inactive, dimeric intermediates have also been identified in the equilibrium unfolding reactions of such enzymes as the dimeric bacterial luciferase, the tetrameric R67 dihydrofolate reductase, the tetrameric β-galactosidase, and the tetrameric phosphofructokinase (*13*−*17*). Interestingly, partially folded and catalytically active intermediate states have yet to be identified in the folding reactions of single- or multi-subunit enzyme systems.

Recently, we began studies on a new model enzyme system, 4-oxalocrotonate tautomerase (4-OT),[1] in order to better understand the interrelationship between protein folding, subunit assembly, and enzyme function (*18*, *19*). 4-OT is a 41 kDa bacterial isomerase that consists of 6 identical 62-amino acid subunits organized into a homo-hexamer and stabilized entirely by noncovalent interactions (*20*, *21*). Our initial equilibrium unfolding studies on 4-OT indicated that the GuHCl-induced equilibrium unfolding behavior of the enzyme was well-modeled by a two-state model involving the folded hexamer and six unfolded monomers and that the folded hexamer was stabilized by 68.7 ± 3.2 kcal·mol^{-1}

† This work was supported by Duke University and the Research Corp. P.S. was supported in part by funds from an NIH-sponsored Biological Training Program at Duke University.

* Correspondence should be addressed to this author at the Department of Chemistry, Box 90346, Duke University, Durham, NC 27708-0346. Tel: 919-660-1547, Fax: 919-660-1605, E-mail: mfitz@chem.duke.edu.

[1] Abbreviations: 4-OT, 4-oxalocrotonate tautomerase; 2-HM, 2-hydroxymuconate; GuHCl, guanidine hydrochloride; Bpa, *p*-benzoyl-L-phenylalanine; ANS, 1-anilinonaphthalene-8-sulfonic acid; UV-CD, ultraviolet-circular dichroism; SEC, size-exclusion chromatography; RP-HPLC, reversed-phase high-performance liquid chromatography; ESI-MS, electrospray ionization mass spectrometry; MALDI-MS, matrix-assisted laser desorption ionization mass spectrometry; F_{app}, apparent fraction of unfolded enzyme; ΔG_{H_2O}, free energy change of unfolding in the absence of denaturant.

10.1021/bi011872w CCC: $22.00
Published on Web 03/08/2002

compared to the unfolded monomer at pH 8.5 (*18*). In contrast, the GuHCl-induced equilibrium unfolding properties of 4-OT at pHs 6.0 and 7.4 were best described by at least a three-state unfolding process involving significant population of partially folded intermediate state(s).

High-resolution structural studies on 4-OT have shown that the enzyme's six subunits are organized as a trimer of dimers in the native enzyme complex (*21*). Biochemical studies on 4-OT have also shown the key catalytic residues (i.e., Pro-1 and Arg-11 from one subunit and Arg-39 from an adjacent subunit) reside within a dimer unit (*22*, *23*). The organization of the subunits in 4-OT, the location of the active site in 4-OT, and the results of our earlier GuHCl-induced equilibrium unfolding studies of 4-OT at low pH suggested that a dimeric state of 4-OT with some degree of catalytic activity might be stabilized under acidic solution conditions. The primary goal of this work was to determine if such a partially folded intermediate state of 4-OT was stabilized at low pH and to acquire information about the catalytic and structural properties of such a state if it existed.

Here we utilize SEC, far-UV-CD, and catalytic activity measurements to study the pH-induced equilibrium unfolding of 4-OT. We find that at least three different states of the enzyme are populated in the pH range from 1.5 to 10.1. The native hexamer is the predominant species in solution at pHs $\geq$6.2; a folded dimeric state of 4-OT is the predominant species in solution at pH 4.8; and a largely denatured state is populated under strongly acidic conditions (pHs $\leq$3.1). GuHCl-induced equilibrium unfolding studies on 4-OT at pH 4.8 suggest that the folded 4-OT dimer populated at this pH has a defined structure that is stabilized by 11.7 ± 0.1 kcal·mol^{-1}. The results of biophysical studies on a fluorescent analogue of the enzyme, 4-OT(F50Y), and the results of UV photo-cross-linking studies on a synthetically derived 4-OT analogue, 4-OT(P1Bpa), are also reported here. The results of these studies on 4-OT(F50Y) and 4-OT(P1Bpa) provide important information about the 4-OT dimer structure. We also find that the dimer did not display any significant catalytic activity.

MATERIALS AND METHODS

Materials. Sodium dihydrogen phosphate, disodium hydrogen phosphate, *N*,*N*-diisopropylethylamaine, and sequencing grade *S. aureus* V-8 protease were purchased from Sigma-Aldrich. GuHCl was obtained from OmniPur, and ANS was purchased from Molecular Probes. The *tert*-butoxycarbonyl (Boc) L-amino acids were purchased from Peptide Institute, Inc., and Novabiochem, and the *tert*-Boc-Arg(tosyl)OCH_2 PAM resin was obtained from Applied Biosystems. The 2-(1*H*-benzotriazol-1-yl)-1,1,3,3-tetramethyluronium hexafluorophosphate (HBTU) was obtained from Quantum Biotechnologies. Neat trifluoroacetic acid (TFA) (biograde) was purchased from Halocarbon, and spectroscopic grade dimethylformamide was obtained from J. T. Baker. Anhydrous HF (UHP) was purchased from Matheson Gas. HPLC grade acetonitrile was obtained from Mallinckrodt. The 2-hydroxymuconate (2-HM) was a gift from Professor Christian P. Whitman (University of Texas at Austin). All other chemicals were of reagent grade or better.

General Methods and Instrumentation. Analytical and preparative reversed-phase high-performance liquid chromatography (RP-HPLC) separations were performed on a Rainin instrument consisting of a Dynamax SD-200 Solvent Delivery System and a Dynamax variable-wavelength UV/Visible absorbance detector. Analytical RP-HPLC was performed on a C_{18} Vydac column (0.46 $\times$ 15.0 cm, 300 Å) at a flow rate of 1 mL/min. Preparative RP-HPLC was performed on a C_{18} Vydac column (2.2 $\times$ 12.0 cm, 300 Å) at a flow rate of 10 mL/min. All RP-HPLC separations were performed using linear gradients of Buffer B in Buffer A (Buffer A = 0.1% TFA in water, and Buffer B = 90% acetonitrile in water containing 0.09% TFA). Detection for analytical and preparative separations was at 214 and 230 nm, respectively. SEC was also performed on the Rainin system. SEC separations were carried out utilizing a Superdex 75 HR 10/30 column (Pharmacia Biotech) at a flow rate of 1 mL/min. The mobile phase in our SEC experiments was 20 mM sodium phosphate buffer in which the pH was adjusted to that of the sample. Detection for SEC experiments was at 214 nm.

Electrospray ionization mass spectra were obtained using a PE-Sciex API 150EX electrospray ionization mass spectrometer (ESI-MS). Typically, samples were diluted into 40% Buffer B in Buffer A, and then infused directly into the mass spectrometer at a flow rate of 10 μL/min using a Harvard Syringe pump. Matrix-assisted laser desorption/ionization mass spectrometry (MALDI-MS) was performed using a Voyager DE Biospectrometry Workstation (Perseptive Biosystems, Inc.). All spectra were acquired in the positive-ion mode. MALDI-MS samples were prepared by the dried droplet method using α-cyano-4-hydroxycinnamic acid (4-HCCA) as the matrix. All UV/vis absorbance data were collected using a Hewlett-Packard 8452A Diode Array UV/vis Spectrophotometer and a quartz cuvette (1 cm). All far-UV-CD measurements were acquired at 25 °C using a Jasco-710 Spectropolarimeter and a bandwidth of 0.5 nm. Far-UV-CD spectra were obtained using a 1 cm quartz cuvette for enzyme solutions $<$10 μM, and using a 0.5 cm quartz cuvette for more concentrated enzyme solutions. Steady-state fluorescence measurements were acquired at 25 °C using an SLM 48000S Spectrofluorometer (Spectronics Instruments, Inc., Rochester, NY) equipped with a 450 W xenon arc lamp for excitation and PMT detection. All fluorescence measurements were obtained using a 0.5 cm quartz cuvette. Excitation was at 390 nm for experiments involving ANS, and at 280 nm for experiments involving 4-OT(F50Y). Enzyme concentrations were determined using the Waddell method (*24*). All GuHCl concentrations were determined by refractive index measurements at 25 °C (*25*).

Protein Purification. Two pET24a plasmids, one containing the wild-type 4-OT gene and one containing the 4-OT-(F50Y) gene, were kindly provided by Professor Christian P. Whitman (University of Texas at Austin). Wild-type 4-OT and 4-OT(F50Y) were overexpressed and isolated from *Epicurian coli* BL21-Gold(DE3) cells as described elsewhere (*18*). Ultimately, each enzyme construct was purified from the crude cell lysate by preparative RP-HPLC. Pure fractions, as determined by ESI-MS, were combined, frozen, and lyophilized to a dry white powder.

pH-Induced Equilibrium Unfolding Experiments. Protein samples were prepared either by dilution of unfolded 4-OT

sample solutions containing 5 M GuHCl and 50 mM phosphate buffer (pH 7.4) into 20 mM phosphate buffers of varying pH or by dilution of folded 4-OT sample solutions containing 50 mM phosphate buffer (pH 7.4) into 20 mM phosphate buffers of varying pH. In both cases, the final protein solutions were equilibrated overnight at room temperature prior to their analysis by SEC, far-UV-CD, fluorescence, or catalytic activity. The final concentration of protein in the samples used in the SEC experiments was 45 μM for wild-type 4-OT and 22 μM for 4-OT(F50Y), and 1 mL of each protein solution was loaded onto the SEC column. The final concentration of protein in the samples used for far-UV-CD, fluorescence, and catalytic activity analyses was 5 μM. Our results were not dependent on whether the protein samples were prepared from folded or unfolded stocks of the enzyme.

The catalytic activity of 4-OT was assayed using the substrate 2-HM according to previously reported protocols (*18*). Briefly, catalytic rates were determined by monitoring the rate of product formation. This was accomplished by measuring the change in absorbance at 232 nm in 1 s intervals over a 5 s time period, and then performing a linear least-squares analysis in order to obtain the initial rate in AU/s. All activity measurements were recorded in 20 mM phosphate buffers at pHs that matched that of the sample. In these activity assays, the final concentration of the enzyme ranged from 1 nm to 1 μM, and the concentration of the 2-HM substrate ranged from 25 to 500 μM.

GuHCl-Induced Equilibrium Unfolding Experiments. The protein solutions used to generate the GuHCl-induced equilibrium unfolding curves in this work were prepared by mixing two different stock solutions of enzyme. One stock contained the folded enzyme in 50 mM phosphate buffer (pH 4.8, 6.0, or 7.4), and the other contained the unfolded enzyme in 50 mM phosphate buffer (pH 4.8, 6.0, or 7.4) containing 5 M GuHCl. Both of these stock solutions were prepared by dilution (always $\geq$10-fold) of the same concentrated, 5 M GuHCl denatured 4-OT solution. The folded and unfolded stock solutions were mixed in appropriate ratios in order to generate a series of equimolar enzyme solutions with GuHCl concentrations ranging from 0.1 to 4.0 M. The pH of each solution was adjusted to within $\pm$0.1 of the desired pH by the addition of small amounts (<1% v/v) of a 1 N sodium hydroxide solution. All the protein solutions used in the equilibrium unfolding experiments were equilibrated overnight at room temperature before analysis.

In this work, GuHCl-induced equilibrium unfolding curves were obtained on 4-OT(F50Y) at pH 6.0 and 7.4 using catalytic activity, far-UV-CD, and intrinsic fluorescence. GuHCl-induced equilibrium unfolding curves were also obtained on wild-type 4-OT and 4-OT(F50Y) at pH 4.8 by far-UV-CD. Far-UV-CD denaturation curves were obtained by monitoring the CD signal of the protein at 222 nm. Typically, the ellipticity value at 222 nm for each protein solution was measured in 0.5 s intervals for 30 s, and an average value was determined. Fluorescence denaturation curves were obtained on 4-OT(F50Y) by monitoring the fluorescence intensity at 306 nm, the emission maximum from Y50. Raw data from far-UV-CD, intrinsic fluorescence, and catalytic activity measurements were normalized by converting the raw signal to an apparent fraction of unfolded enzyme (F_{app}) according to eq 1 (*26*):

$$F_{app} = \frac{S - S_F}{S_F - S_U} \tag{1}$$

where S is the far-UV-CD signal at 222 nm, fluorescence intensity at 306 nm, or catalytic rate at a given GuHCl concentration; and S_F and S_U are the respective signals of the folded and unfolded forms of the enzyme at each GuHCl concentration. In our experiments, S was linearly dependent on the GuHCl concentration in both the folded and unfolded baselines, so linear extrapolations from these baselines were used to estimate S_F and S_U values in the transition region.

Normalized data were appropriately fit to the following two-state (folded and unfolded) models:

$$H \leftrightarrow 6M \tag{2}$$

$$T \leftrightarrow 3M \tag{3}$$

$$D \leftrightarrow 2M \tag{4}$$

where H, T, and D represent folded 4-OT hexamer, trimer, and dimer (respectively); and M represents unfolded monomer. The equilibrium constants for the unfolding reactions in eqs 2−4 can be written, respectively, in the following forms:

$$K_{6,eq} = \frac{6[M]^6}{[P_{tot}]_M - [M]} \tag{5}$$

$$K_{3,eq} = \frac{3[M]^3}{[P_{tot}]_M - [M]} \tag{6}$$

$$K_{2,eq} = \frac{2[M]^2}{[P_{tot}]_M - [M]} \tag{7}$$

where $[P_{tot}]_M$ is the total protein concentration in terms of monomer and [M] is the concentration of unfolded monomer. If the apparent fraction of unfolded enzyme, F_{app}, is defined as $[M]/[P_{tot}]_M$, the equilibrium constants in eqs 5−7 can be rewritten, respectively, in the following forms:

$$K_{6,app} = \frac{6F_{app}^{\ 6}[P_{tot}]_M^5}{1 - F_{app}} \tag{8}$$

$$K_{3,app} = \frac{3F_{app}^{\ 3}[P_{tot}]^2}{1 - F_{app}} \tag{9}$$

$$K_{2,app} = \frac{2F_{app}^{\ 2}[P_{tot}]_M}{1 - F_{app}} \tag{10}$$

where $K_{6,app}$, $K_{3,app}$, and $K_{2,app}$ are the apparent equilibrium constants at each GuHCl concentration according to the models in eqs 2−4. For a two-state unfolding process and at moderate to high denaturant concentrations, the apparent free energy of unfolding (ΔG_{app}) is linearly dependent on the molar concentration of the denaturant according to eq 11 (*26, 27*):

$$\Delta G_{app} = \Delta G_{H_2O} + m_g[\text{denaturant}] \tag{11}$$

where ΔG_{app} is the apparent free energy of unfolding at a particular denaturant concentration and at standard state (1 M hexamer), m_g is the constant of proportionality ($\delta\Delta G_{app}/\delta$[denaturant]), and ΔG_{H_2O} is the free energy change of unfolding in the absence of denaturant.

In equilibrium studies of the chemical denaturant-induced unfolding of proteins, thermodynamic parameters are typically obtained by using a nonlinear least-squares analysis to fit the dependence of F_{app} upon the chemical denaturant concentration. This global fitting of the data requires an expression for F_{app} in terms of [denaturant], $[P_{tot}]_M$, ΔG_{H_2O}, and m_g. Such an expression can be easily derived in the case of the D ↔ 2M model using eqs 10 and 11. However, such an expression for F_{app} is not easily derived in the case of the T ↔ 3M and H ↔ 6M models due to the high order of eqs 8 and 9. This ultimately precludes the use of standard nonlinear least-squares analysis programs based on the Marquardt−Levenberg algorithm to fit the data in our denaturation curves to these models. Therefore, in our two-state analyses of the equilibrium unfolding curves in this work, we extracted ΔG_{H_2O} and m_g values from the data by using eqs 8−11 and the expression $\Delta G_{app} = -RT \ln(K_{app})$ to convert F_{app} values in the transition region of each denaturation curve to ΔG_{app} values. These ΔG_{app} values were then used to generate global ΔG_{app} vs [GuHCl] plots for each model. Ultimately, a linear least-squares analysis of these global plots of the data yielded m_g values and extrapolated ΔG_{H_2O} values for each model.

1-Anilinonaphthalene-8-sulfonic Acid (ANS) Binding. Wild-type 4-OT was equilibrated in 20 mM phosphate buffers at pHs 1.5, 4.8, and 8.5 at a protein concentration of 5 μM. Aliquots from a 1 mM stock solution of ANS were diluted into each 4-OT solution to a final ANS concentration of 25 μM (5:1 molar excess of ANS compared to 4-OT). After 20 h of equilibration at room temperature, emission spectra were recorded from 420 to 600 nm using a bandwidth of 1 nm. The excitation wavelength was 390 nm.

Total Chemical Synthesis and Purification of 4OT(P1Bpa). 4-OT(P1Bpa) was prepared by total chemical synthesis using manual solid-phase peptide synthesis (SPPS) methods and in situ neutralization protocols for *tert*-butyloxycarbonyl (Boc) chemistry as described elsewhere (*28*, *29*). In this 4-OT analogue, the photoreactive amino acid *p*-benzoyl-L-phenylalanine (Bpa) replaced Pro-1 in the wild-type sequence. Synthesis was initiated on Boc-L-Arg(tosyl)OCH_2 PAM resin. Side protection was as follows: Arg(Tos), Asp(OcHex), Glu(OcHex), His(Bom), Lys(2-Cl-Z), Ser(Bzl), and Thr(Bzl) where Tos is tosyl, OcHex is cyclohexyl, Bom is *tert*-butyloxymethyl, 2-Cl-Z is 2-chlorobenzyloxycarbonyl, and Bzl is benzyl. Side chain deprotection and cleavage of the peptide from the resin were carried out by treatment with anhydrous HF at 0 °C for 1 h; and *p*-cresol was used as a scavenger in the deprotection and cleavage reaction. Following HF removal, the crude peptide was precipitated and washed with cold anhydrous diethyl ether, dissolved in a minimal amount of 70% acetonitrile containing 0.1% TFA, diluted with water, frozen, and lyophilized. The desired product was purified from the crude peptide mixture by preparative RP-HPLC using a 40−60% linear gradient of Buffer B in Buffer A. Pure RP-HPLC fractions, as judged by ESI-MS analysis, were pooled, frozen, and lyophilized to a dry, white solid.

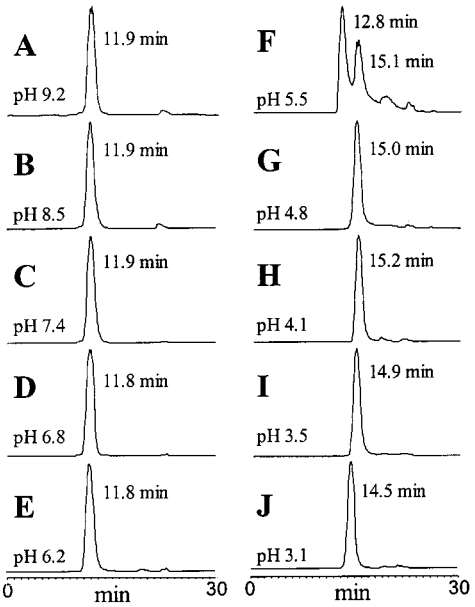

FIGURE 1: SEC elution profiles of 4-OT samples equilibrated in 20 mM phosphate buffers ranging in pH from 9.2 to 3.1. In each case, the composition and pH of the mobile phase matched those of the sample.

4-OT(P1Bpa) UV Photo-cross-linking and Peptide Mapping. For all photo-cross-linking experiments, RP-HPLC-purified 4-OT(P1Bpa) was dissolved in a 50 mM phosphate buffer containing 5 M GuHCl, and then diluted ≥100-fold into 20 mM phosphate buffers at pH 1.5, 4.8, and 8.5. The 4-OT(P1Bpa) samples were equilibrated in each buffer for at least 2 h at room temperature. UV photo-cross-linking of the refolded material was carried out by irradiating the solutions with UV light (355 nm) from a hand-held UVGL-55 ultraviolet lamp (Ultraviolet Products, Upland, CA) as describe elsewhere (*30*). Solutions were irradiated for 30 min, and then analyzed by analytical RP-HPLC using a linear gradient of 40−80% Buffer B in Buffer A. The major peaks from RP-HPLC analysis were collected and identified by their mass using ESI-MS. The material collected from the major peaks in each chromatogram was frozen and lyophilized to a dry white solid. This solid was ultimately redissolved in 20 mM phosphate buffer (pH 7.4) and digested for 20 h at 37 °C with *S. aureus* V-8 protease. After digestion, aliquots were diluted 1:10 into a saturated matrix solution and analyzed by MALDI-MS.

RESULTS

Size-Exclusion Chromatography (SEC). SEC analyses were performed on 10 different wild-type 4-OT samples that were equilibrated in 20 mM phosphate buffers ranging in pH from 3.1 to 9.2. The SEC elution profiles recorded for these 4-OT samples are shown in Figure 1. Only one major peak at approximately 12 min was detected in the SEC chromatograms recorded at pHs 6.2−9.2. One major peak was also detected in the SEC chromatograms recorded at pHs 3.1−4.8. At pHs 4.8 and 4.1, the retention time of this major peak was approximately 15 min, whereas at pHs 3.5 and 3.1 the retention times of the major peak were measurably lower, 14.9 and 14.5 min (respectively). Two major peaks (one at 13 min and one at 15 min) were detected in the SEC chromatogram obtained at pH 5.5.

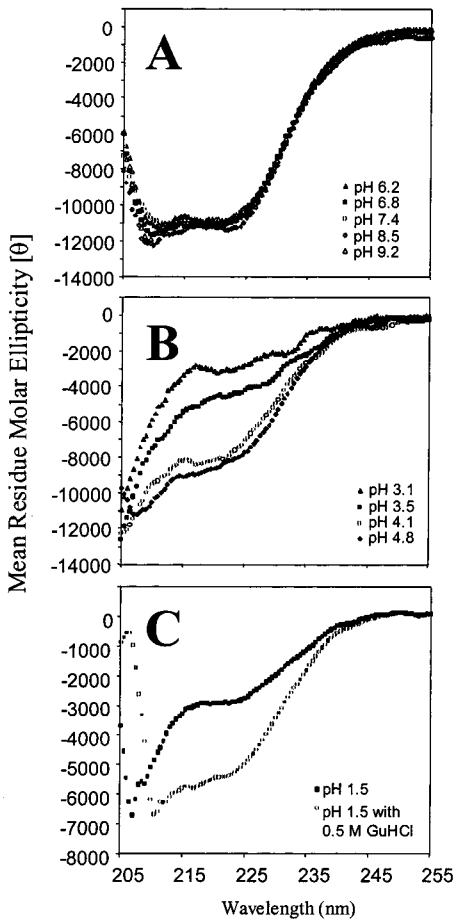

FIGURE 2: Far-UV-CD of 4-OT samples in 20 mM phosphate buffers ranging in pH from (A) 9.2 to 6.2, (B) 4.8 to 3.1, and (C) at pH 1.5. All spectra were recorded at 25 °C at an enzyme concentration of 5 μM.

No attempt was made to assign the retention times in our SEC experiments to oligomeric states of 4-OT due to the enzyme's aberrant behavior on conventional sizing columns (*20*). However, it is noteworthy that material isolated from the 12 min peaks in the SEC elution profiles recorded at pHs 7.4, 8.5, and 9.2 was catalytically competent with catalytic properties essentially identical to those reported for the wild-type enzyme under native solution conditions (20 mM phosphate buffer, pH 7.4). Far-UV-CD spectra collected on material isolated from these 12 min peaks were also consistent with far-UV-CD spectra previously recorded for the wild-type enzyme (see Figure 2A). Therefore, we reasoned that 4-OT's native, homo-hexameric complex eluted at approximately 12 min under the chromatographic conditions (i.e., flow rate and column) employed in our experiments. It was also difficult to determine the oligomeric state of the late eluting peak in the SEC elution profiles obtained at pHs 5.5, 4.8, 4.1, 3.5, and 3.1 due to 4-OT's aberrant behavior in SEC experiments. However, we have observed that unfolded 4-OT monomer (i.e., 4-OT denatured in 2.5 M GuHCl) irreversibly binds to the Superdex column used in our SEC experiment. Therefore, we do not believe that the material in the late eluting peaks observed in our SEC analyses at lower pHs is monomeric.

In each SEC analysis, the same amount of material was injected on the sizing column (1 mL of a 45 μM solution of 4-OT). Greater than 95% of the total material loaded on the column at pHs 6.2, 7.4, 8.5, and 9.2 was recovered in the eluant from the sole 12 min peak observed in the chromatograms recorded at these pHs. In our size-exclusion analyses at pHs 4.8, 4.1, 3.5, and 3.1, approximately 80% of the total material loaded on the column was recovered in the eluant from the sole 15 min peak in the SEC chromatograms recorded at these pHs. Approximately 40−60% of the total material loaded on the column at pH 5.5 was recovered in the eluant collected from the two major peaks observed in the chromatogram recorded at this pH. We attributed the protein losses in our SEC analyses at lower pHs to unfolded monomer that may form in the mobile phase and irreversibly bind to the column during the chromatographic separation.

Far-UV-CD Spectroscopy and Catalytic Activity Measurements. The material that eluted in the major peaks in the SEC chromatograms shown in Figure 1 was isolated and further characterized by far-UV-CD spectroscopy. Far-UV-CD spectra recorded for material isolated in the 12 min peaks of the SEC chromatograms obtained at pH 6.2, 6.8, 7.4, 8.5, and 9.2 were very similar and essentially identical to far-UV-CD spectra previously reported for the native hexamer (Figure 2A).

Far-UV-CD spectra recorded for material isolated from the major peaks in the SEC chromatograms recorded at pHs 3.1, 3.5, 4.1, and 4.8 are shown in Figure 2B. The far UV-CD spectra that we recorded at these lower pHs were slightly different from each other and significantly different from spectra recorded for the native enzyme (i.e., see the pH 7.4 spectrum shown in Figure 2A). In particular, the magnitudes of the mean molar ellipticity values between 210 and 230 nm decreased significantly at these lower pHs. For example, at pHs 4.8, 4.1, 3.5, and 3.1, mean molar ellipticity values at 222 nm (a value that can be correlated to the α-helical content of a polypeptide chain) were only 30−70% of the value measured for the wild-type enzyme.

Interestingly, it was not possible to isolate material exclusively from the 12.8 and 15.1 min peaks in the SEC chromatogram recorded at pH 5.5. Once it was collected, material that was isolated from these peaks rapidly equilibrated to a mixture of species with an SEC elution profile equivalent to that initially obtained for the sample. Therefore, it was not possible to record a far-UV-CD spectrum of material exclusively from the 13 or 15 min peaks observed in our SEC analysis of 4-OT at pH 5.5.

The working pH range of the sizing column used in our SEC experiments extended from pH 3 to 12; therefore, it was not possible to generate SEC elution profiles for 4-OT samples at pHs <3.0. However, we did record far-UV-CD spectra of 4-OT at pH 1.5 (see Figure 2C). The magnitudes of the mean molar ellipticity values that we recorded between 210 and 230 nm for the 4-OT sample at pH 1.5 were only slightly decreased from those recorded for the enzyme at pH 3.1. It is also noteworthy that the far-UV-CD spectrum of the 4-OT sample at pH 1.5 changed significantly upon addition of 0.5 GuHCl to the buffer (see Figure 2C). Notably, no changes in the far-UV-CD spectra recorded at pHs 4.8 and 8.5 were detected upon the addition of 0.5 M GuHCl to 4-OT samples at these pHs.

To better understand the pH-dependent folding properties of 4-OT, we directly measured the far-UV-CD signal at 222 nm and the catalytic activity of 15 different 4-OT samples that were equilibrated in 20 mM phosphate buffers ranging

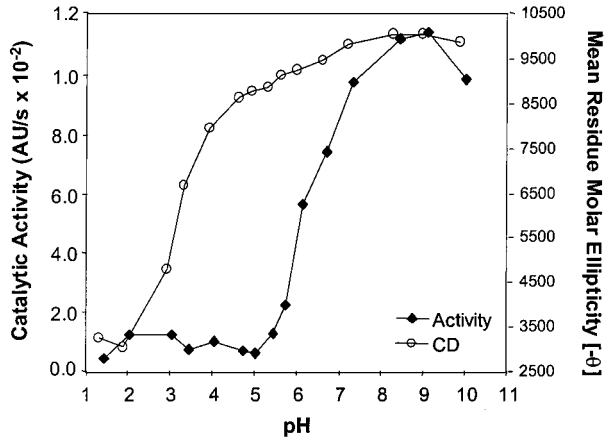

FIGURE 3: pH dependence of the far-UV-CD signal at 222 nm (closed diamonds) and the catalytic activity (open circles) for 4-OT. The catalytic rate measurements are the initial rates obtained in an enzyme assay containing 1 nM enzyme and 100 μM 2-HM substrate.

in pH from 1.5 to 10.1 (Figure 3). The catalytic rate measurements in Figure 3 were the initial rates obtained in assay buffer containing 100 μM 2-HM and enzyme from a 5 μM stock solution that was diluted 5000-fold. Our initial rate measurements and the magnitude of the enzyme's far-UV-CD signal were at a maximum at pHs 8.5 and 9.2. A small decrease in both the enzyme's catalytic efficiency and the far-UV-CD signal was detected at pH 10.1. A dramatic decrease in the enzyme's catalytic activity was observed between pH 8.5 and 5.8, and the enzyme was essentially inactive at pHs $\leq$4.8. In contrast to the large decrease in catalytic activity that was observed between pHs 8.5 and 4.8, there was only a small decrease in the enzyme's far-UV-CD signal in this same pH range. The far-UV-CD signal recorded for the 4-OT solution at pH 4.8 was approximately 80% of that recorded for the 4-OT solution at pH 8.5. Only below pH 4.1 was there a dramatic decrease in the enzyme's far-UV-CD signal.

The catalytic rate measurements recorded in Figure 3 were obtained using a final enzyme concentration of 1 nM in each assay buffer. To better evaluate the enzyme's activity at pH 4.8, we also increased the concentration of enzyme in our assays at this pH. Using micromolar concentrations of the enzyme in the assay, we were able to determine k_{cat} and K_M values of 2.1 s^{-1} and 14 μM (respectively) for 4-OT at pH 4.8. The k_{cat} and K_M values for the enzyme under native solution conditions (pH 7.4) have been reported to be on the order of 3000 s^{-1} and 50 μM (*20*). We also observed that the specific activity of the enzyme increased with increasing protein concentration. These results suggest the presence of concentration-dependent equilibria. The small amount of catalytic activity in our 4-OT samples at pH 4.8 could be explained by the presence of a small amount ($\sim$0.1%) of native hexamer present in equilibrium with the dimer.

GuHCl-Induced Equilibrium Unfolding of Wild-Type 4-OT at pH 4.8. The GuHCl-induced equilibrium unfolding of 4-OT was studied in 20 mM phosphate buffer at pH 4.8 using the enzyme's far-UV-CD signal at 222 nm as a structural probe. The far-UV-CD denaturation curves recorded at three different protein concentrations ranging from 10 to 90 μM are shown in Figure 4A. The normalized data (see Materials and Methods) are shown in Figure 4B. The data in Figure 4 show that the midpoint of the unfolding transition was shifted to higher GuHCl concentrations with increasing protein concentration, indicating that at least two different oligomeric states of the enzyme are populated in the equilibrium unfolding reaction of 4-OT at pH 4.8.

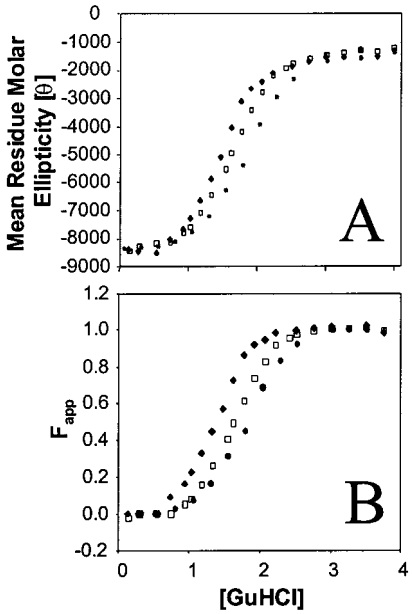

FIGURE 4: GuHCl-induced equilibrium unfolding data for 4-OT at pH 4.8 and 25 °C obtained by far-UV-CD at 222 nm. (A) Raw data obtained at enzyme concentrations of 10 μM (closed diamonds), 30 μM (open squares), and 90 μM (closed circles). (B) Normalized data obtained at the same enzyme concentrations as in (A).

Thermodynamic parameters, ΔG_{H_2O} and m_g, were obtained from normalized CD denaturation curves using three different two-state models as described under Materials and Methods. The normalized data in Figure 4 were globally fit to models that assumed the only species populated at equilibrium were hexamer and monomer; trimer and monomer; and dimer and monomer (see Figure 5). The ΔG_{H_2O} and m_g values we calculated from the global fits of the data shown in Figure 5 were ultimately used to generate theoretical denaturation curves at each enzyme concentration. Theoretical denaturation curves generated for each two-state model are plotted together with the normalized CD data we recorded experimentally in Figure 6A−C. A visual inspection of the data in Figure 6 reveals that the experimental data are in best agreement with the theoretical curves generated using a two-state model involving a folded dimer and two unfolded monomers (Figure 6C). Using this model, average values for ΔG_{H_2O} and m_g were calculated (in terms of dimer) to be 11.7 $\pm$ 0.1 kcal·mol^{-1} and 3.3 $\pm$ 0.1 kcal·mol^{-1}·M^{-1}.

ANS Binding Studies with 4-OT. The fluorescence properties of ANS can be used to identify the presence of exposed hydrophobic regions and "molten-globule" conformations of proteins (*31*, *32*). The fluorescence emission spectra recorded for ANS in 4-OT solutions buffered at pHs 1.5, 4.8, and 8.5 are shown in Figure 7. The relative fluorescence from ANS in the presence of 4-OT was greatest at pH 1.5 with an emission maximum at about 490 nm. At pH 4.8, the emission maximum from ANS was blue-shifted to about 470 nm, and approximately 40% less intense than the maximum at pH 1.5. The fluorescence intensity of ANS was lowest in the

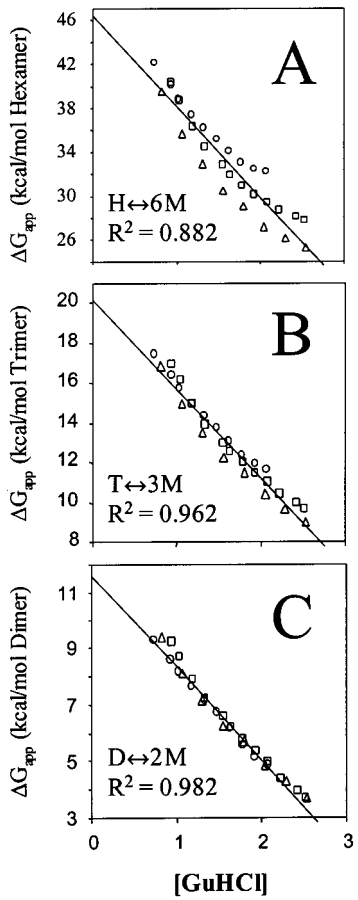

FIGURE 5: Global fit of GuHCl-induced equilibrium unfolding data for 4-OT at pH 4.8. Data were obtained at enzyme concentrations of 10 μM (open circles), 30 μM (open squares), and 90 μM (open triangles) and analyzed according to two-state models involving (A) folded hexamer and six unfolded monomers, (B) folded trimer and three unfolded monomers, and (C) folded dimer and two unfolded monomers. For each model, the solid line represents the best-fit line from our global linear least-squares analysis of the data at all three enzyme concentrations.

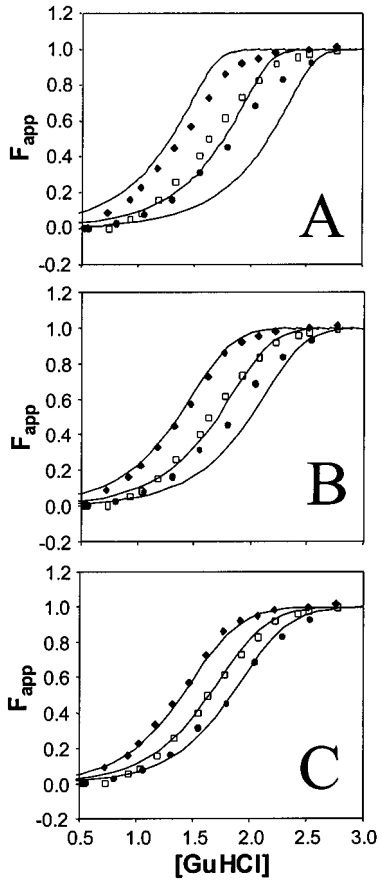

FIGURE 6: GuHCl-induced equilibrium unfolding curves of 4-OT at pH 4.8 and 25 °C as monitored by far-UV-CD at 222 nm and fit to two-state models involving (A) folded hexamer and six unfolded monomers, (B) folded trimer and three unfolded monomers, and (C) folded dimer and two unfolded monomers. Denaturation curves were obtained at enzyme concentrations of 10 μM (closed diamonds), 30 μM (open squares), and 90 μM (closed circles) and were normalized to F_{app}. For each model, the solid lines represent the theoretical denaturation curves generated using the ΔG_{H_2O} and m_g values that were determined by global analysis of the data (see Figure 5).

4-OT sample at pH 8.5 (the emission maximum was at about 490 nm and was approximately 70% less intense than the emission maximum at pH 1.5).

Biophysical Characterization of 4-OT(F50Y). There are no Trp or Try residues in the primary amino acid sequence of 4-OT. As part of the work described here, we have carried out a series of biophysical studies on a fluorescent analogue 4-OT(F50Y). We reasoned that the conservative Phe to Tyr mutation at position 50 in the 62 amino acid polypeptide chain of 4-OT would have minimal impact on the folding and functional properties of the enzyme and that the Tyr mutation in this analogue would be a useful structural probe for the C-terminal region of the polypeptide chain of 4-OT. This C-terminal region makes important dimer−dimer contacts in the native hexamer. The SEC elution profiles, the far-UV-CD spectra, and the catalytic parameters (i.e., k_{cat} and K_M values) recorded for the 4-OT(F50Y) samples at pHs 4.8 and 8.5 were essentially identical to those recorded for the wild-type enzyme at these pHs (data not shown). It is also noteworthy that the pH-induced equilibrium unfolding of 4-OT(F50Y) was also essentially identical to that of the wild-type enzyme as judged by the protein's catalytic activity and far-UV-CD signal at 222 nm (data not shown).

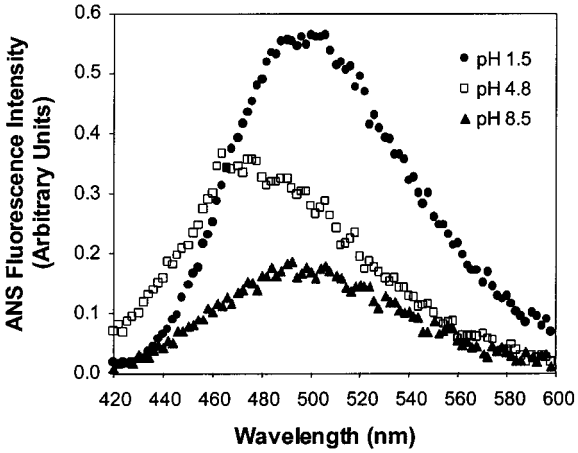

FIGURE 7: ANS fluorescence in the presence of 4-OT after 20 h at 25 °C. Fluorescence emission spectra were obtained at pH 1.5 (closed circles), pH 4.8 (open squares), and pH 8.5 (gray triangles). Excitation was at 390 nm.

The GuHCl-induced equilibrium unfolding of 4-OT(F50Y) was monitored in 50 mM phosphate buffers at pHs 7.4, 6.0, and 4.8 using catalytic activity measurements with 2-HM, far-UV-CD measurements at 222 nm, and fluorescence

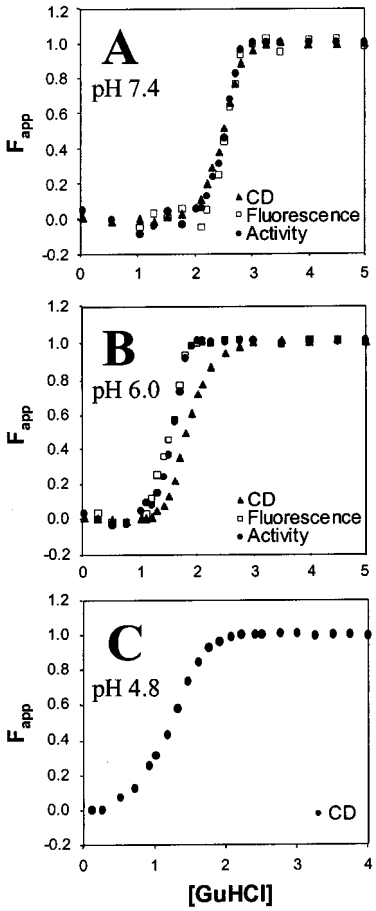

FIGURE 8: Normalized data for the GuHCl-induced equilibrium unfolding of 4-OT(F50Y) at (A) pH 7.4, (B) pH 6.0, and (C) pH 4.8. The data at pHs 7.4 and 6.0 were obtained using catalytic activity (closed circles), far-UV-CD (gray triangles), and intrinsic fluorescence at 306 nm (open squares). The data at pH 4.8 were obtained using far-UV-CD (closed circles).

emission measurements at 306 nm (280 nm excitation). Shown in Figure 8 are the normalized CD, activity, and fluorescence data as a function of [GuHCl]. At pH 7.4, a single, cooperative unfolding transition was observed for each structural probe (i.e., activity, CD, and fluorescence). The unfolding curves recorded with each structural probe at pH 7.4 (see Figure 8A) were also coincident; and the midpoint of each denaturation curve was approximately 2.5 M GuHCl. The normalized data in each 4-OT(F50Y) denaturation curve at pH 7.4 were fit to an apparent two-state model involving folded hexamer and six unfolded monomers (see Materials and Methods) in order to extract ΔG_{H2O} and m_g values. The values we obtained are summarized in Table 1.

In contrast to the results obtained for the 4-OT(F50Y) construct at pH 7.4, the activity, CD, and fluorescence denaturation curves recorded for the 4-OT(F50Y) construct at pH 6.0 were not coincident (Figure 8B). While the activity and fluorescence unfolding transitions for this 4-OT(F50Y) were highly cooperative and essentially identical to each other, the unfolding transition recorded using the enzyme's far-UV-CD signal as a structural probe at pH 6.0 was significantly more shallow and shifted to higher GuHCl concentrations. We have previously observed similar results using catalytic activity and far-UV-CD to monitor the GuHCl-induced equilibrium unfolding of the wild-type enzyme at pH 6.0 (*18*). It is noteworthy that the fluorescence

Table 1: Two-State Analysis of the Guanidine-Induced Equilibrium Unfolding of 4-OT(F50Y) at 25 °C

pH	structural probe	ΔG_{H_2O} (kcal·mol^{-1})[a]	m_g (kcal·mol^{-1}·M^{-1})[a]
7.4	activity	73.7 ± 1.5 (65.0 ± 2.2)	14.9 ± 0.6 (13.8 ± 0.8)
	CD	66.0 ± 1.6 (61.7 ± 3.8)	11.9 ± 0.7 (11.8 ± 1.4)
	fluorescence	73.0 ± 5.9	14.3 ± 2.3
	average	70.9 ± 4.3 (63.4 ± 3.3)	13.7 ± 1.6 (12.8 ± 1.4)
4.8	CD	11.4 ± 0.1 (11.7 ± 0.1)	3.6 ± 0.1 (3.3 ± 0.1)

[a] Results were obtained at pH 7.4 using a two-state model involving folded hexamer and six unfolded monomers, and at pH 4.8 using a two-state model involving folded dimer and two unfolded monomers. Values obtained using each structural probe are reported with the standard error from linear least-squares analysis. Average values from three replicate experiments are reported with a standard deviation. Values in parentheses represent results previously determined in ref *18* for the wild-type enzyme under similar conditions.

denaturation curve recorded for 4-OT(F50Y) is identical to the activity denaturation curve and not the CD denaturation curve for this construct.

The far-UV-CD transition we recorded for the GuHCl-induced equilibrium unfolding of 4-OT(F50Y) in 50 mM phosphate buffer at pH 4.8 is shown in Figure 8C. It was not possible to record activity and fluorescence denaturation curves for 4-OT(F50Y) at pH 4.8. Similar to our observations with the wild-type enzyme, the substantially reduced catalytic properties of the 4-OT(F50Y) precluded our ability to record an activity denaturation curve for this analogue at pH 4.8. Also, the absence of a change in the fluorescence signal of 4-OT(F50Y) upon unfolding in GuHCl at pH 4.8 precluded our ability to record a fluorescence denaturation curve for this analogue at pH 4.8. However, the CD denaturation curve exhibited a single, cooperative unfolding transition with a transition midpoint at approximately 1.4 M GuHCl. The normalized data were fit to an apparent two-state unfolding model involving folded dimer and two unfolded monomers (see Materials and Methods) in order to extract values for ΔG_{H_2O} and m_g. The values we obtained are summarized in Table 1.

pH-Induced Equilibrium Unfolding and UV Photo-Cross-Linking of 4-OT(P1Bpa). To obtain structural information about the N-terminal region of the polypeptide chain of 4-OT at pH 4.8, we undertook studies of 4-OT(P1Bpa). We have shown that the photoreactive properties of the Bpa moiety in this analogue can be used to probe the structural integrity of 4-OT's N-terminus (*30*). As part of this work, pure 4-OT(P1Bpa) was refolded in 20 mM phosphate buffers at pH 1.5, 4.8, and 8.5 and equilibrated overnight. The SEC elution profiles and the far-UV-CD spectra recorded for the 4-OT(P1Bpa) samples at pHs 1.5, 4.8, and 8.5 were nearly identical to those recorded for the wild-type enzyme at these pHs (data not shown). The 4-OT(P1Bpa) protein samples in each 20 mM phosphate buffer (pH 1.5, 4.8, and pH 8.5) were also exposed to 355 nm light from a hand-held UV lamp for 30 min. The RP-HPLC chromatograms obtained for each 4-OT(P1Bpa) sample after the 30 min cross-linking reaction are shown in Figure 9. ESI-MS analysis of material eluting under the major peaks at approximately 15 and 17 min in each chromatogram confirmed the presence of monomer (6947.0 amu) and photo-cross-linked dimer (13 894 amu), respectively. Based on a peak area analysis of the RP-HPLC chromatograms, 61% of the material was photo-cross-linked

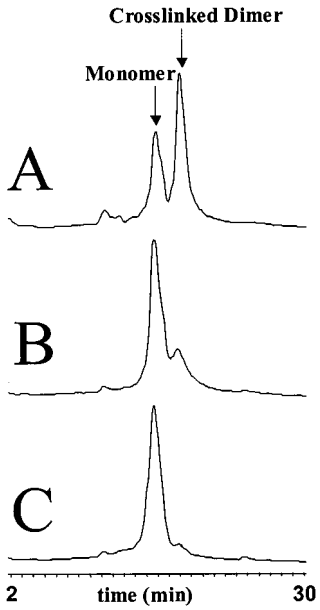

FIGURE 9: RP-HPLC analysis of photo-cross-linked 4-OT(P1Bpa) (A) at pH 8.5, (B) at pH 4.8, and (C) at pH 1.5. ESI-MS was used to identify the peaks eluting at approximately 15 and 17 min as the 62-amino acid monomer unit of 4-OT and a photo-cross-linked dimer of 4-OT, respectively.

at pH 8.5 to form a covalently linked dimer species, 26% of the material was photo-cross-linked at pH 4.8 to from a covalently linked dimer species, and <5% of the material was photo-cross-linked at pH 1.5 to from a covalently linked dimer species.

Material isolated from the monomer and cross-linked dimer peaks in the RP-HPLC chromatograms in Figure 9 was also subjected to proteolytic digestion with V-8 protease. MALDI-MS analyses of material isolated from the monomer peaks in each chromatogram in Figure 9 yielded intense peptide ion signals at *m*/*z* values of approximately 827, 1083, 2040, and 1185 after digestion with V-8 protease. These ion signals were consistent with the formation of peptide fragments containing 4-OT(P1Bpa) residues 56−62, 45−55, 1−9, and 26−44 (respectively). Significantly, no ion signals that could be assigned to photo-cross-linked peptide fragments were observed in the MALDI mass spectra recorded for the V-8 protease digests of the monomeric material that we isolated.

MALDI-MS analyses of material isolated from the cross-linked dimer peaks in the chromatograms shown in Figure 9A,B yielded intense peptide ion signals at *m*/*z* values of approximately 827, 1083, 2040, and 2135 after digestion with V-8 protease. The ion signals at *m*/*z* values of 827, 1083, and 2040 were similar to those observed above in the MALDI-MS analysis of the monomer material after it was digested with V-8 protease; and, as above, they can be assigned to peptide fragments containing 4-OT(P1Bpa) residues 56−62, 45−55, and 26−44. Interestingly, the ion signal at *m*/*z* 2135 was unique to MALDI-MS spectra recorded for the photo-cross-linked dimer isolated from the chromatograms in Figure 9A,B after V-8 protease digestion. This ion signal at *m*/*z* 2135 can be attributed to the photo-cross-linked peptide product shown schematically in Figure 10C. Unfortunately, no ion signals were detected in the MALDI analysis of material isolated from the small cross-linked dimer peak in the chromatogram shown in Figure 9C.

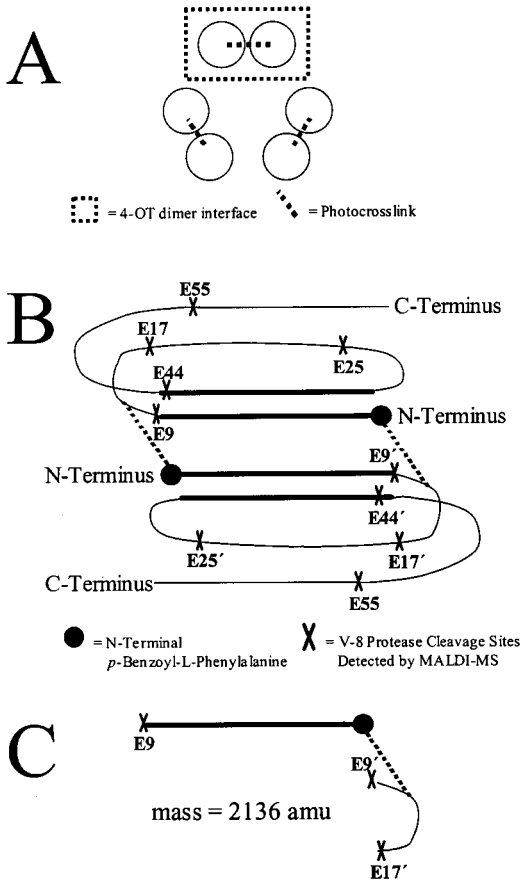

FIGURE 10: (A) Schematic representation of the 4-OT hexamer showing the organization of the subunits into a trimer of dimers. (B) Schematic representation of the major intersubunit, β-sheet interface in 4-OT showing the glutamic acid, E, sites cleaved in our V-8 protease digestions. (C) Schematic representation of the photo-cross-linked peptide fragment detected in our MALDI analysis of our V-8 digests of photo-cross-linked dimers.

This was presumably due to the limited amount of material that could be isolated from this small peak.

DISCUSSION

Native-like Hexamer at pH 6.2−10.1. The results of our SEC studies and far-UV-CD analyses of 4-OT indicate that the there were no gross changes in the enzyme's higher order structure from pH 6.2 to 10.1. The far-UV-CD spectra we recorded for 4-OT samples at pH 6.2, 6.8, 7.4, 8.5, 9.2, and 10.1 were essentially identical to each other; and the SEC elution profiles recorded for the enzyme in this pH range included only one major peak with a retention time of approximately 12 min. Attempts to characterize the native oligomeric structure of 4-OT (i.e., the enzyme's oligomeric state in buffer at pH 7.4) have yielded variable results. For example, the enzyme was classified as an octamer by native gel electrophoresis (*33*); and it was classified as a pentamer by SEC and analytical ultracentrifugation (*20*). However, more recent studies of the enzyme by "native" electrospray ionization mass spectrometry and by X-ray crystallography have indicated that 4-OT likely adopts a homo-hexameric structure under native solution conditions (i.e., pH 7.4) (*34*, *21*). Therefore, since no gross structural changes in the enzyme were detected in our SEC and far-UV-CD studies at pHs 6.2−10.1, we reasoned that 4-OT folded into a nativelike homo-hexameric structure in this pH range.

While no major changes in the overall three-dimensional structure of 4-OT were detected at pHs 6.2−10.1, significant differences in the catalytic activity of the enzyme were observed in this pH range. The enzyme's catalytic activity was at a maximum between pH 8.5 and 9.2 but decreased at pHs >9.2 and at pHs <8.5 (see Figure 3). These results are consistent with the bell-shaped pH−rate profiles for the kinetic parameters (k_{cat} and K_M) of 4-OT that have been reported in earlier studies of the enzyme's catalytic properties (*22*, *23*).

A Stable 4-OT Dimer at pH 4.8. The SEC elution profiles, the far-UV-CD spectra, and the far-UV-CD denaturation curves recorded for 4-OT at pH 4.8 are consistent with the enzyme adopting a partially folded dimeric structure at this pH. The far-UV-CD spectrum obtained at pH 4.8 indicates that there is significant α-helical content in the 62-amino acid polypeptide chain of 4-OT. Based on the magnitude of the molar ellipticity at 222 nm, the polypeptide chain is approximately 20% α-helical (*35*). This is close to the α-helical content (∼25%) previously reported for the native homo-hexameric structure of 4-OT. Unfortunately, it was not possible to unambiguously assign the multimeric state of 4-OT at pH 4.8 using the SEC data collected in this work due to the enzyme's aberrant behavior on conventional sizing columns (*20*). However, the results of our GuHCl-induced equilibrium unfolding studies on 4-OT at pH 4.8 provide strong evidence that the partially folded 4-OT structure populated at this pH is a stable dimer.

Our main evidence that a stable 4-OT dimer is the predominant species in solution at pH 4.8 comes from the protein concentration dependence of the unfolding transitions that we observed in our GuHCl-induced equilibrium unfolding studies of 4-OT at pH 4.8. The unfolding transitions that we recorded were well described by a two-state model involving folded dimer and unfolded monomer (see Figure 6C). Two-state models involving other folded, multimeric states of the enzyme (e.g., hexamer or trimer) and unfolded monomer did not fit our GuHCl-induced equilibrium unfolding data at pH 4.8. Our analysis of the far-UV-CD denaturation data at pH 4.8 using a two-state model involving folded dimer and unfolded monomer indicated that the dimer was stabilized by 11.7 ± 0.1 kcal/mol under standard conditions (1 M dimer). It is noteworthy that the thermodynamic stability of the 4-OT dimer is consistent with the thermodynamic stability of other dimeric proteins of similar size. For example, the homo-dimeric Arc repressor structure, which consists of 2 identical 53-amino acid polypeptide chains, is stabilized by approximately 11 kcal/mol (*36*).

Our two-state analysis of the partially folded 4-OT dimer populated at pH 4.8 also yielded an m_g value of 3.3 kcal·mol^{-1}·M^{-1}. The magnitude of the m_g values is dependent on the amount a protein's solvent-accessible surface area is changed upon denaturation; and it has been shown that m_g values can be related to the size of a protein. The m_g value that we calculated for the partially folded 4-OT structure at pH 4.8 is consistent with that expected for a folded 4-OT dimer (i.e., a 124-amino acid protein structure). Based on an average, estimated m_g value per residue of 0.026 ± 0.007 kcal·mol^{-1}·M^{-1}, one would expect an m_g value of 3.3 kcal·mol^{-1}·M^{-1} for a folded 4-OT dimer (*37*).

Structural Properties of 4-OT Dimer. Some insight into the structural features of the 4-OT dimer can be gleaned from the results of our ANS binding experiments (Figure 6). ANS is known to bind to exposed hydrophobic surfaces in proteins, particularly when proteins exhibit a "molten-globule" conformation (*31*, *32*). Frequently, this "molten-globule" state of a protein may be induced under increasingly acidic conditions (*4*, *38*). Our results indicate that ANS binding to 4-OT was strongest at pH 1.5, indicative of a denatured state of the enzyme with structural features characteristic of a "molten-globule" state. ANS binding to 4-OT was weakest at pH 8.5, as would be expected for a well-structured, compact, folded protein. Interestingly, the relative binding affinity of ANS to 4-OT appeared to be intermediate at pH 4.8. This suggests that the overall structure of the stable dimer at pH 4.8 is more folded and compact than a "molten-globule" state, but less ordered than the native 4-OT hexamer.

The fluorescence properties of Y50 in 4-OT(F50Y) were also a useful structural probe of the partially folded 4-OT dimer identified in this work. Significant differences in the fluorescence intensity of Tyr-50 was observed upon the GuHCl-induced unfolding of 4-OT(F50Y) at pHs 6.0 and 7.4; and it was possible to record fluorescence denaturation curves at these pHs. However, at pH 4.8, no difference in the fluorescence intensity of Tyr-50 was observed; and a fluorescence denaturation curve could not be recorded. Our inability to record a GuHCl denaturation at pH 4.8 using Tyr-50 fluorescence as a structural probe suggests that the C-terminal region of 4-OT's polypeptide chain is unstructured and/or solvent-exposed in the 4-OT dimer that is populated at pH 4.8.

Some additional insight into the structure of the partially folded 4-OT dimer that is populated at pH 4.8 was provided by photo-cross-linking experiments with a synthetically derived analogue, 4-OT(P1Bpa). The photoreactive Bpa residue in this analogue replaces Pro-1 that lies at the major monomer−monomer interface located within each dimer subunit in the native structure of 4-OT (see Figure 10). We have previously demonstrated that this analogue can be used to map subunit interactions involving the N-terminal region of 4-OT's polypeptide chain (*30*). Significantly, we found that the photo-cross-linking results obtained with the 4-OT(P1Bpa) analogue at pH 4.8 and 8.5 were similar in that high yields of photo-cross-linked dimer, 26% and 61% (respectively), were detected at each pH. The higher photo-cross-linking yield at pH 8.5 can be attributed to the high thermodynamic stability of the hexamer at pH 8.5 (approximately 69 kcal/mol). It is also especially noteworthy that the results of our peptide mapping experiments localized the site(s) of the covalent cross-link(s) in the photo-cross-linked dimers formed at pH 4.8 and 8.5 to the same 8-amino acid region of 4-OT's polypeptide chain. These results suggest that there are similarities in the enzyme's overall three-dimensional structure at pHs 4.8 and 8.5, particularly near the photo-cross-linked site in 4-OT(P1Bpa). The results of our MALDI-based peptide mapping experiments indicate that the major photo-cross-linking site in 4-OT(P1Bpa) is positioned at the end of an intersubunit β-sheet region in 4-OT. Our results suggest that this intersubunit β-sheet is formed and oriented in a native-like fashion in the folded 4-OT dimer structure at pH 4.8.

Catalytic Properties of 4-OT Dimer. The K_M value we recorded for the 4-OT dimer at pH 4.8 was similar in magnitude to that reported for the enzyme under native conditions, whereas the k_{cat} value we recorded for the dimer

at pH 4.8 was approximately 3 orders of magnitude less than that recorded for the enzyme under native conditions (pH 7.4) (*20*). The similarities in these K_M values suggest that the substrate binding properties of 4-OT, which involve two arginine residues from adjacent subunits, are not grossly perturbed at pH 4.8. This is consistent with the structural data above (i.e., our photo-cross-linking data which suggest the intersubunit β-sheet region in the native structure of 4-OT being well formed and native like in the folded dimer at pH 4.8).

In earlier studies on the catalytic properties of 4-OT, it was determined that Pro-1 was the general base catalyst and that this residue had an unusually low pK_a (pK_a = 6.4) due to a low dielectric constant in the active site (*22, 23*). The lack of any significant catalytic activity in the 4-OT dimer populated at pH 4.8 is likely due to the protonation state of Pro-1 at this pH (i.e., it is protonated). The small amount of activity that we detected for the 4-OT dimer at pH 4.8 could be attributed to a small population of molecules bearing an unprotonated Pro-1 residue at the N-terminus of 4-OT. This could be due to a change in the chemical properties of the active site in the dimer (i.e., an altered dielectric constant) or due to the presence of a small population of folded hexamer in which Pro-1 was unprotonated. The latter is consistent with our observation that the specific activity of the enzyme was concentration-dependent, as such a small population of folded hexamer could potentially be in equilibrium with the dimer at pH 4.8. Sedimentation equilibrium studies are in progress to investigate the biophysical properties of this equilibrium.

In conclusion, our results indicate that the native hexamer and at least one partially folded intermediate state of 4-OT, a folded dimer with little or no catalytic activity, is populated in the enzyme's pH-induced equilibrium unfolding. The folded dimer is the predominant species in solution at pH 4.8, and GuHCl-induced equilibrium unfolding studies on 4-OT at pH 4.8 suggest that this folded dimer contains well-defined higher order structure that is stabilized by approximately 11.7 $\pm$ 0.1 kcal·mol^{-1}. Moreover, the results of far-UV-CD studies and photo-cross-linking experiments indicate that this folded 4-OT dimer populated at pH 4.8 contains many "native-like" interactions found in the native 4-OT hexamer. However, the 4-OT dimer at pH 4.8 was not catalytically competent. This is despite the fact that there are gross structural similarities between the dimer and the native hexamer and that the major catalytic residues in 4-OT are contained in the dimer structure. These results are similar to those reported in protein folding studies of other enzyme systems (*6*−*17*). Partially folded intermediate states populated in an enzyme's unfolding reaction are not generally catalytically competent as critical properties of enzyme active sites are usually disrupted in such partially folded structures.

NOTE ADDED IN PROOF

Prakash et al. recently identified a catalytically competent oligomeric intermediate of bovine liver catalase (*39*).

ACKNOWLEDGMENT

We recognize David C. Evans and Dr. Bassam M. Nakhle for their initial observation that 4-OT's retention time on a Superdex column was significantly increased at low pH.

REFERENCES

1. Jaenicke, R. (1987) *Prog. Biophys. Mol. Biol. 49*, 117−237.
2. Kim, P. S., and Baldwin, R. L. (1990) *Annu. Rev. Biochem. 59*, 631−660.
3. Matthews, C. R. (1993) *Annu. Rev. Biochem. 62*, 653−683.
4. Chamberlain, A. K., and Marqusee, S. (2000) *Adv. Protein Chem. 53*, 283−323.
5. Jaenicke, R., and Lilie, H. (2000) *Adv. Protein Chem. 53*, 329−397.
6. Wang, H. R., Zhang, T., and Zhou, H. M. (1995) *Biochim. Biophys. Acta 1248*, 97−106.
7. Prajapati, S., Bhakuni, V., Babu, K. R., and Jain, S. K. (1998) *Eur. J. Biochem. 225*, 178−184.
8. Tsou, C. L. (1986) *Trends Biochem. Sci. 11*, 427−429.
9. Tsou, C. L. (1993) *Science 262*, 380−381.
10. Herold, M., and Kirschner, K. (1990) *Biochemistry 29*, 1907−1913.
11. Smith, C. J., Clarke, A. R., Chia, W. N., Irons, L. I., Atkinson, T., and Holbrook, J. J. (1991) *Biochemistry 30*, 1028−1036.
12. Risse, B., Stempfer, G., Rudolph, R., Mollering, H., and Jaenicke, R. (1992) *Protein Sci. 1*, 1699−1709.
13. Clark, A. C., Sinclair, J. F., and Baldwin, T. O. (1993) *J. Biol. Chem. 268*, 10773−10779.
14. Zhuang, P., Eisenstein, E., and Howell, A. E. (1994) *Biochemistry 33*, 4237−4244.
15. Nichtl, A., Buchner, J., Jaenicke, R., Rudolph, R., and Scheibel, T. (1998) *J. Mol. Biol. 282*, 1083−1091.
16. Deville-Bonne, D., Le Bras, G., Teschner, W., and Garel, J. (1989) *Biochemistry 28*, 1917−1922.
17. Teschner, W., and Garel, J. (1989) *Biochemistry 28*, 1912−1916.
18. Silinski, P., Allingham, M. J., and Fitzgerald, M. C. (2001) *Biochemistry 40*, 4493−2502.
19. Nakhle, B. M., Silinski, P., and Fitzgerald, M. C. (2000) *J. Am. Chem. Soc. 122*, 8105−8111.
20. Chen, L. H., Kenyon, G. L., Curtin, F., Harayama, S., Bembenek, M. E., Hajipour, G., and Whitman, C. P. (1992) *J. Biol. Chem. 267*, 17716−17721.
21. Roper, D. I., Subramanya, H. S., Shingler, V., and Wigley, D. B. (1994) *J. Mol. Biol. 243*, 799−801.
22. Stivers, J. T., Abeygunawardana, C., Mildvan, A. S., Hajipour, G., and Whitman, C. P. (1996) *Biochemistry 35*, 814−823.
23. Czerwinski, R. M., Harris, T. K., Johnson, W. H., Jr., Legler, P. M., Stivers, J. T., Mildvan, A. S., and Whitman, C. P. (1999) *Biochemistry 38*, 12358−12366.
24. Waddell, W. J. (1956) *J. Lab. Clin. Med. 48*, 311−314.
25. Pace, C. N. (1986) *Methods Enzymol. 131*, 266−279.
26. Pace, C. N. (1975) *CRC Crit. Rev. Biochem.*, 1−43.
27. Santoro, M. M., and Bolen, D. W. (1992) *Biochemistry 31*, 4901−4907.
28. Fitzgerald, M. C., Chernushivech, I., Standing, K. G., Kent, S. B. H., and Whitman, C. P. (1995) *J. Am. Chem. Soc. 117*, 11075−11080.
29. Schnolzer, M., Alewood, P., Jones, A., Alewood, D., and Kent, S. B. H. (1992) *Int. J. Pept. Protein Res. 40*, 180−193.
30. Moss, J. A., Silinski, P., and Fitzgerald, M. C. (2001) *Fresenius J. Anal. Chem. 369*, 252−257.
31. De Filippis, V., de Laureto, P. P., Toniutti, N., and Fontana, A. (1996) *Biochemistry 35*, 11503−11511.
32. Semisotonov, G. V., Rodionova, N. A., Razgulyaev, O. I., Uversky, V. N., Gripas, A. F., and Gilmanshin, R. I. (1991) *Biopolymers 31*, 119−128.
33. Harayama, S., Rekik, M., Ngai, K. L., and Ornston, L. N. (1989) *J. Bacteriol. 171*, 6251−6258.
34. Fitzgerald, M. C., Chernushivech, I., Standing, K. G., Whitman, C. P., and Kent, S. B. H. (1996) *Proc. Natl. Acad. Sci. U.S.A. 93*, 6851−6856.
35. Chen, Y., Yang, J. T., and Chau, K. H. (1974) *Biochemistry 13*, 3350−3359.
36. Schildbach, J. F., Milla, M. E., Jeffrey, P. D., Raumann, B. E., and Sauer, R. T. (1995) *Biochemistry 34*, 1405−1412.
37. Myers, J. K., Pace, N. C., and Scholtz, J. M. (1995) *Protein Sci. 4*, 2138−2148.

38. Staniforth, R. A., Giannin, S., Bigotti, M. G., Cutruzzolà, F., Travaglini-Allocatelli, C., and Brunori, M. (2000) *J. Mol. Biol. 297,* 1231−1244.

39. Prakash, K., Prajapati, S., Ahmad, A., Jain, S. K., and Bhakuni, V. (2002) *Protein Sci. 11,* 46−57.

BI011872W